Title

Impact of CO2 injection on wettability of coal at elevated pressure and temperature

Authors

Zhu, Chuanjie

Wan, Jiamin

Tokunaga, Tetsu K

et al.

Publication Date

2019-12-01

DOI

10.1016/j.ijggc.2019.102840

Peer reviewed

Impact of CO_2 injection on wettability of coal at elevated pressure and temperature

Chuanjie Zhu [a], Jiamin Wan [b], Tetsu K. Tokunaga [b], Na Liu [a], Baiquan Lin [a], Hourong Wu [c]

[a] Faculty of Safety Engineering, China University of Mining and Technology, Xuzhou, Jiangsu, 221116, China; [b] Earth and Environmental Sciences Area, Lawrence Berkeley National Laboratory, Berkeley, CA, 94720, USA; [c] Technology Center, Sichuan Coal Industry Group LLC, Chengdu, Sichuan, 610091, China.

Abstract: Injection of carbon dioxide (CO_2) into coal seams has been demonstrated as an effective technology for enhanced methane recovery and CO_2 storage. However, the impacts of the geochemical reactions between CO_2 and coal on the wettability of coal pore surfaces, which influences immiscible multiphase displacement, are not yet well understood. We studied wettability alterations of coal surfaces resulting from reactions with gas, liquid and supercritical (sc)CO_2 under varied pressure (1-141 bar) and temperatures (~25 - 60 °C) through measuring static and dynamic contact angles with anthracite coal plates. We found that reactions with gas CO_2 only slightly changed the wettability of coal surfaces from water-wet to intermediate-wet with static contact angles from ~60˚ to 70°-90°. However, reactions with liquid and scCO_2 altered the coal surfaces to strongly CO_2-wet, with the contact angles up to 115-180°. We also found that both static and dynamic contact angles increase significantly with increasing pressure. Temperature affects the contact angles reversely especially under supercritical pressure conditions. These relationships of contact angles with pressure and temperature may be explained by the CO_2 density dependence on pressure and temperature.

Keywords: Coalbed methane, Carbon dioxide, Wettability, Supercritical CO_2, Contact angle, Temperature, Pressure.

1 Introduction

The technology of carbon dioxide (CO_2) enhanced coalbed methane recovery (CO_2-ECBM, a method involving CO_2 injection and storage into coal seams) has been advanced greatly since it was proposed by Puri and Lee (Puri and Yee, 1990) and Gunter (Gunter, et al., 1997). CO_2 injection into coal seams involves several complex

steps, including the mixture of gas and liquid advection and diffusion in fractures or cleats, and CO_2 competitive adsorption with water and methane, which have been extensively studied by many researchers (Busch and Gensterblum, 2011; Masoudian, 2016; Mukherjee and Misra, 2018). Given the presence of water in CBM reservoirs, wettability of coal surfaces is a fundamental factor controlling CO_2 injection, adsorption, and sequestration (Arif, et al., 2017).

The wettability of a solid surface is commonly characterized by static and dynamic water contact angles. The wettabilities of varieties of rock and mineral surfaces in CO_2 and brine systems relevant to CO_2 storage and enhanced oil and gas recoveries have been studied, including substrates such as shales, mica, quartz, phyllosilicate, and calcite (Bikkina, 2011; Chen, et al., 2015; Jung and Wan, 2012; Pan, et al., 2018; Wan, et al., 2014; Wan, et al., 2018). Wettability of coals with respect to water and other fluids has also been reported (Eissler and Holde, 1962; Jańczuk, et al., 1988; Kilau, 1993; Saghafi, et al., 2014). Kaveh et al. (Kaveh, et al., 2011) measured the contact angles of synthetic flue gas (80/20 of N_2/CO_2 mixture) and pure CO_2 on a Warndt Luisenthal coal (high volatile bituminous (hvBb) medium rank coal). They reported that the static contact angles (SCA) linearly increased with pressure, and the coal surface became hydrophobic under pressures higher than 85 bar at 45 °C. Sakurovs and Lavrencic (Sakurovs and Lavrencic, 2011) measured contact angles in a coal-water-scCO_2 system at 40 °C and pressures up to 150 bar and found that contact angles for the coals ranging between 80° to 100°, except for one coal with a contact angle of 115°. Mahoney et al. (Mahoney, et al., 2017) measured contact angles (H_2O phase) in a water–CO_2–anthracite coal system for pressures ranging from atmospheric pressure to 140 bar. They reported that the coals remained water-wet with contact angles of 85° at atmospheric pressure, while the coal sample became CO_2-wet as the pressure increased above 2.6 bar. Recently, Arif et al. (Arif, et al., 2016; Arif, et al., 2017) measured the CO_2-wettability of coals from low to high ranks using the pendant drop tilted plate technique. They found that the high-rank coals were strongly CO_2-wet, medium-rank coals are weakly CO_2-wet, and low-rank coals are intermediate-wet at typical coal reservoir conditions. In addition, the CO_2-wettability of coals increased with pressure and salinity, and decreased with temperature irrespective of the coal rank.

However, most of the previous researches focused on static contact angles only except Arif et al (2016), and the measurements were conducted with single CO_2 phase (gas or supercritical phase),

despite the fact that CO_2 injection into coalbeds usually encounters different reservoir temperatures and pressure, so that the CO_2 may exist as gas, liquid or supercritical phases. In order to examine wettability (For consistent, the single word “wettability” in the present work means water wettability) over the range of typical reservoir conditions, we measured SCAs on coals at different temperatures and pressures. Given that coalbeds commonly contain abundant water, dynamic contact angles (DCAs) were measured by using CO_2 bubbles surrounded by the water in the present work, just as DCAs have been measured on other minerals in many previous studies. This approach mimics CO_2 injection into water-saturated coals, with CO_2 initially displacing water. In Arif et al.’s experiments, water droplets were released into CO_2-saturated coals, such that water is initially displacing CO_2. Thus, the present study includes DCA measurements that are complementary to those of Arif et al.

2 Experiments

2.1 Coal sample and preparation

Although low-rank coals with lower mining value have been considered to be most beneficial for CO_2-ECBM and CO_2 storage (Leung, et al., 2014; White, et al., 2003), in recent years, China has been shutting down many coal mines, some with thin coal seams and many with high-rank coals, because of safety concerns (State Administration of Work Safety et al., (2014). It is worth noting that CO_2 injection into high-rank coals with greater hardness usually does not cause coal and gas outbursts (State Administration of Work Safety, et al., (2006). Therefore, there may be a great potential to inject CO_2 into high-rank coal seams to enhance coalbed methane recovery, and high-rank anthracite coal was collected from a coal mine in China for testing in this study. Proximate analysis results of the coal are shown in Table 1. The pore size distribution and a scanning electron micrograph (SEM) image are shown in Figure 1.

Table 1. Proximate analysis results of the coal sample

Index	Value by mass (%)
Moisture (air dry basis)	2.14
Ash (dry basis)	11.04
Volatile (dry and ash free basis)	5.81
Fixed carbon (dry and ash free basis)	83.8
Maximum vitrinite reflectance (R_{max})	2.41

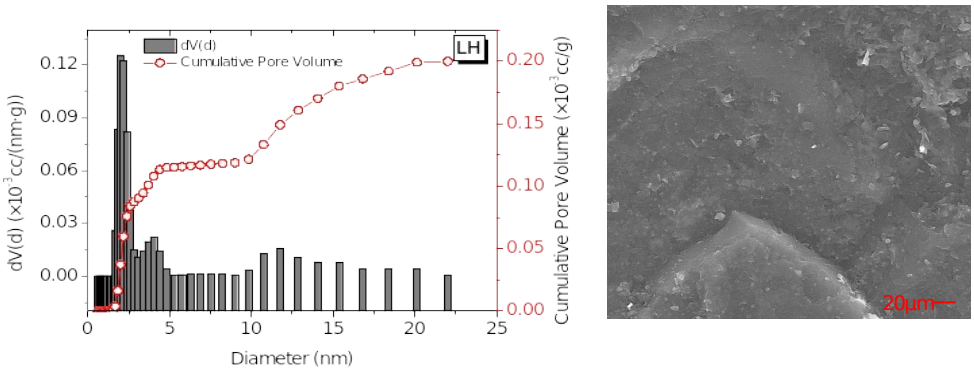

(a) (b)

Figure 1 Pore size distribution and SEM image of the coal sample (not polished). (a) Pore size distribution, (b) SEM image.

There are two different methods to prepare coal substrates. The first method uses high-pressure compressed discs (with artificial surfaces) made from the powdered coal, which may average the surface of the coal substrate with different organic and inorganic compositions (Sun, et al., 2018). However, this method may be more suitable for substrates contacting with air (or other gases) at atmospheric pressure or low pressures. In our study, we also tried to use compressed discs but failed due to coal substrates dissolved gradually in water even at atmospheric pressure. Therefore, we used the other method involving cutting coal slices from large coal blocks. In our experiments, coal samples were cut into square slices with a dimension of ~21 mm × 21 mm ×3-4 mm (thickness).

Surface roughness is one of the important factors influencing the contact angle measurement (Letellier, et al., 2007; Marmur, 2006). Therefore, the surface treatment of the coal sample is very important. However, there is no standard criterion for treating coal surfaces. Siemons et al. and Kaveh et al. polished coal surfaces with a series of abrasive papers of grits from 60 to 1200, followed by polishing with 0.5-μm abrasive alumina powder and a fibrous cloth (Drelich, et al., 1997; Kaveh, et al., 2011; Siemons, et al., 2006).

In our experiments, coal surfaces were polished with a series of silicon carbide sandpapers (220 to 10,000 grit). 220 to 320-grit sandpapers were first used to remove small scratches. Surfaces were finished by use of 400 to 10,000-grit sandpapers in turn for carefully wet polishing (washed with water during the polishing operations). Then the coal samples were dried for at least 72 h at room temperature and then cleaned with Accuduster III 2510 (widely used in surface cleaning) before experiments. The surface roughness was measured using atomic force microscopy (AFM) and

the example AFM images are shown in **Figure 2,** indicating reasonable coal surface roughness. The contact angle of the polished coal substrate with distilled water at atmospheric pressure and temperature is 57±5.2° as shown in **Figure 3**, which indicates that the coal surface is water-wet at atmospheric pressure and room temperature.

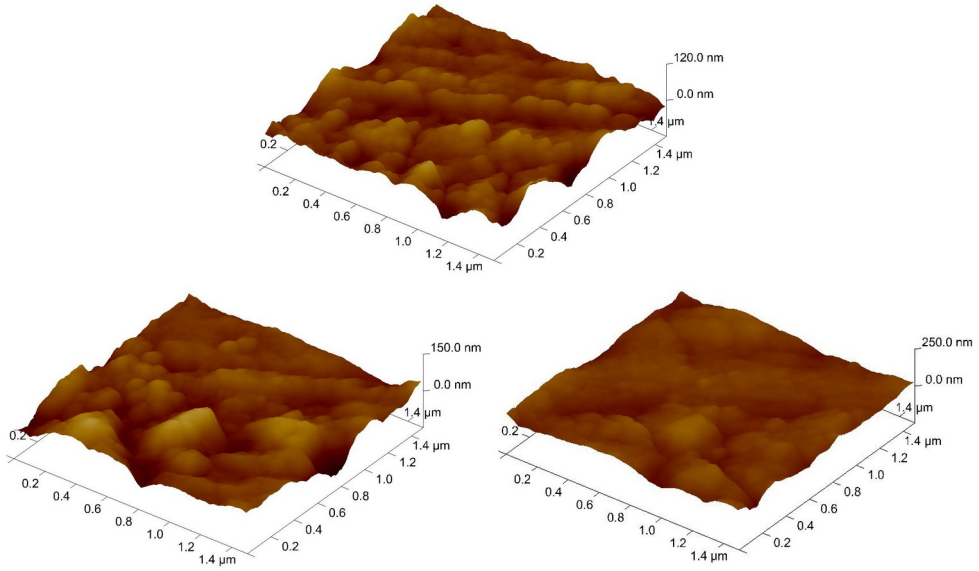

Figure 2 AFM images taken at three different positions of the coal surface after polishing. The arithmetic average (R_a) and root mean square(R_q) roughness of the coal sample are 10.1-14.1 nm and 12.9-19.4 nm, respectively.

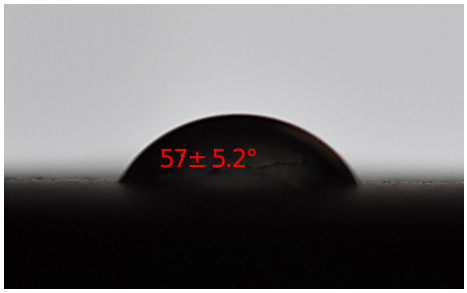

Figure 3 The contact angle of a polished coal substrate with distilled water droplet at atmosphere pressure and room temperature.

2.2 Experiment setup

The experiment system (**Figure 4**) was modified from that used in previous studies (Chen, et al., 2015; Wan, et al., 2014). The maximum working pressure and temperature of the H-P-T (high-pressure and temperature) chamber (IFT-10-P, Core Laboratories) are 10,000 psi and 177 °C, respectively. The chamber has an upper inlet hole connected to a two-stem BuTech manifold (A) with one

stem connected to an ISCO pump (A) providing back pressure and the other stem connected to an exhaust tube to expel CO_2 safely into a fume hood. On the bottom side of the chamber, there is also a lower inlet hole connected to a needle system to generate CO_2 bubbles. The needle system is connected to a 3-way valve by a needle valve used to control the flow rate of CO_2. Another port near the lower inlet hole is connected to a Parr stirred reactor (Parr 4848) via another two-stem BuTech manifold (B) with one stem connected to a water tank for collecting wastewater after experiments. The other ISCO pump (B) was used to provide CO_2 to the Parr stirred reactor.

A stainless plate holds coal substrates near the top side of the chamber. Two high temperature and pressure resistant glass windows installed on opposite sides of the chamber allowing light from an illuminator to pass through the chamber and imaging of droplets (Nikon D7000, 24 fps at resolution of 1920×1080). The temperature in the chamber was controlled by a temperature controller (Digi Sense R/S, used up to 60 ˚C, well below the ~~Max.~~maximum thermocouple input temperature of 1000 °C) which regulated heat circulated from heat lamps with a mixing fan. The whole experiment system was surrounded by thermally insulated walls to maintain environment temperatures controlled by another temperature controller. The space surrounded by thermally insulated walls will be referred to as the thermally insulated box.

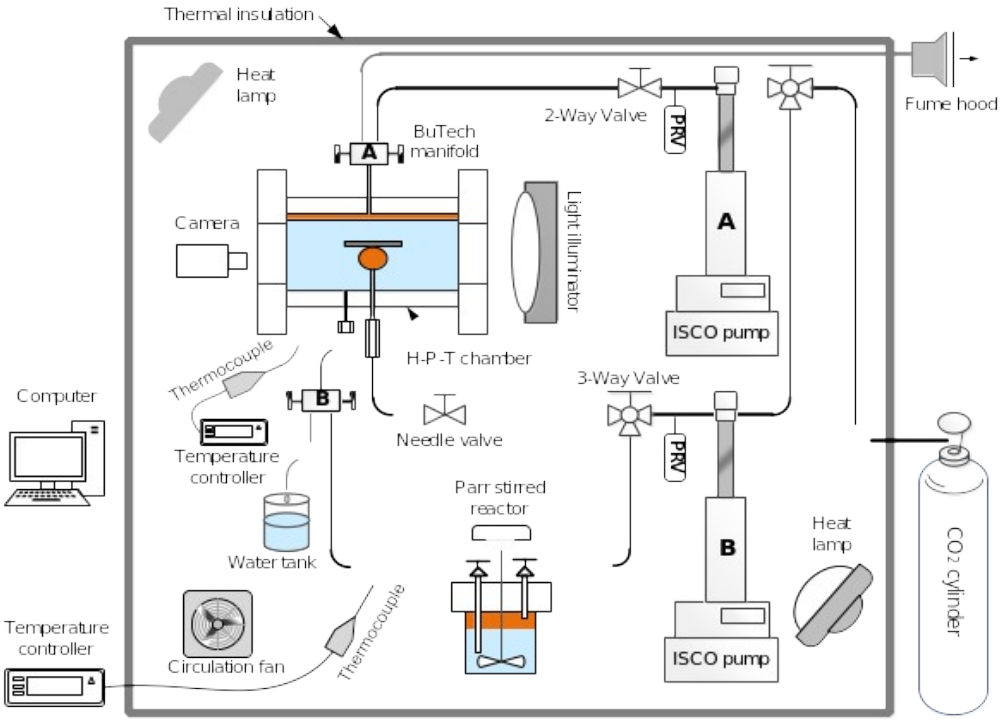

(a)

(b)

Figure 4 High-pressure and temperature contact angle measurement system, (a) Schematic diagram of the system; (b) Photo of the system.

2.3 Experimental procedure

The static and dynamic contact angles can be measured by sessile drop method (Drelich, 2013), pendant drop method (Bhutani, et al., 2012) or captive bubble method (Taggart, et al., 1930). The former two methods are widely used in the contact angle measurement of a liquid droplet resting on a solid surface, while the captive bubble method is more convenient for measuring the contact angle of a CO_2 bubble beneath a solid substrate immersed in a liquid. In our study, the captive bubble method was used. A schematic of the contact angles of gas bubbles beneath a solid substrate is shown in **Figure** 5. The main operations in our experiments are described below.

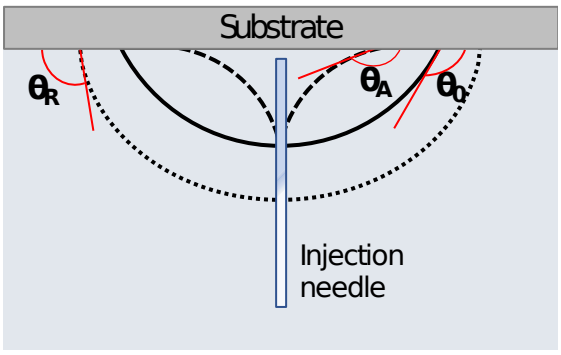

Figure 5. Schematic of the contact angle on a solid substrate immersed in water. Young's contact angle = θ_0, advancing contact angle = θ_A, receding contact angle = θ_R. Usually $\theta_A > \theta_0 > \theta_R$. The left and right advancing or receding contact angles are usually

different and measured individually due to inhomogeneity of physical and chemical properties of the substrate surface. Young's contact angle is impossible to be directly measured, and the static or stable contact angle is measured instead, which usually fluctuates within a range. Note that in this paper we define contact angle as the water contact angle, that is measured through the water phase.

(1) A coal substrate was first clipped onto the stainless plate inside the chamber. The coal substrate was then submersed in high-pressure deionized water (20 bar) for at least 48 h to allow the water to penetrate the coal pores.

(2) The thermally insulated box and the chamber were heated to the desired experimental temperature. The chamber was then filled with CO_2 and pressurized to desired pressure using the ISCO pump (A).

(3) The stirred Parr reactor pre-filled with deionized water was set to the desired temperature and pressurized to slightly higher than the desired pressure using the ISCO pump (B) filled with CO_2. Solubility equilibrium between CO_2 and H_2O was established over a period of 4 h, followed with further stirring for 30 min before injection into the chamber.

(4) The valves between the stirred Parr reactor and the chamber were opened allowing the CO_2-saturated deionized water to flow into the chamber to replace about 90% of the fluid volume of the chamber. During this process, the ISCO pump (A) and (B) were set in constant pressure mode. Further solubility equilibration for ~1 h was performed, considering the pressure difference between injection pressure and back pressure (5 bar at pressures lower than 90 bar, 10 bar at high pressures) between injection pressure and back pressure.

(5) A CO_2 bubble was then released from the stirred Parr reactor via the needle and captured onto the coal substrate. For the dynamic contact angle, the CO_2 bubbles advanced under the pressure difference between the Parr reactor and the H-P-T chamber and receded under the differential pressure between the ISCO pump (B) (pre-depressurized to a lower pressure) and the H-P-T chamber. The bubble expansion and contraction speed (as slow as possible) were controlled by a needle valve. The whole process was recorded by a video, and the images were extracted for contact angle measurements. The static contact bubble was immediately recorded as a photo when contacting the coal substrate (the needle was pulled down and separated from the bubble).

3 Results

3.1 Static contact angles

In our experiments, the contact angles were measured at different combinations of temperatures (~25, 30, 40, 50, and 60 °C) and pressures (1, 21, 41, 61, 91, and 141 bar, absolute pressure), covering gas, liquid and supercritical phases of CO_2 as shown in **Figure 6**. For each experimental point, the contact angle was measured at least 5 times. We also tried to measure the static contact angles at 181 bar, but it is 180° even at 60 °C, suggesting that it was not necessary to measure both the static and dynamic contact angles at such high pressure.

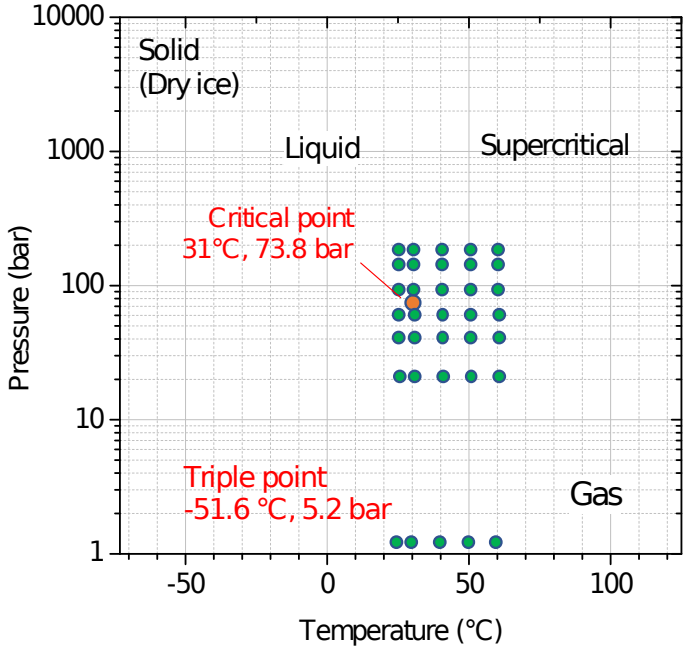

Figure 6. CO_2 phase diagram and a schematic of designed experimental points (green dots) in our experiments.

Figure 7 shows results measured by the static method, i.e. the CO_2 bubble was first generated on the injection needle tip and then contacted the coal surface before the bubble detached and floated to the coal surface. It can be seen that the effect of temperature on the static contact angles at pressures lower than 61 bar (CO_2 in the gas phase) is negligible. However, when the pressure was increased to 91 and 141 bar, the static contact angles decreased significantly with increasing temperature. The static contact angles clearly increased with the increase of pressure, especially for CO_2 transforming from gas to condensed phases. Most of the static contact angles lie between 70° and 90° when the pressures are

between 1 and 61 bar, which indicates that the coal surface is weakly water-wet or intermediate-wet according to Anderson's criteria (Anderson, 1986). Above the critical pressure of CO_2 (73.8 bar), the coal surfaces became strongly CO_2-wet (115-180°), especially below the critical temperature (31.1 ˚C). The static contact angles at 91 bar are ~161° 162° when the temperatures are 25 and 30 °C. They are even higher when the pressure increased to 141 bar (180°). At both higher pressures and temperatures when CO_2 became supercritical, the static contact angles are lower than those in the liquid phase.

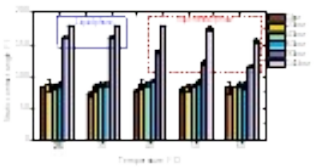

Figure 7 Pressure- and temperature-dependence of static contact angles. Blue dot line – CO_2 in liquid phase, red dash line – CO_2 in supercritical phase, others in gas phase.

3.2 Dynamic contact angles

The dynamic contact angles resulted from the processes of water-advancing (θ_A) or water-receding (θ_R) are important parameters, because that they are in fact the contact angles govern the capillary pressure therefore are relevant during flow. Our DCAs were measured over the same combinations of temperatures and pressures used in our SCA experiments. The DCAs measured on coal substrates in our experiments are shown in **Figure 8**. When the pressure was lower than 61 bar, the advancing and receding contact angles were insensitive to temperature variations. The advancing contact angles varied from 87° to 108° (average values), implying that the coals varied from intermediate-wet to CO_2-wet. The receding contact angles at pressures ≤ 61 bar at a constant temperature are also very close except the ones at 1 bar, which are

slightly lower than those at higher pressures. These receding contact angles lay between 62° and 84° (average values), indicating that the coals became water-wet or intermediate-wet (at 1, 21, 41, 61 bar).

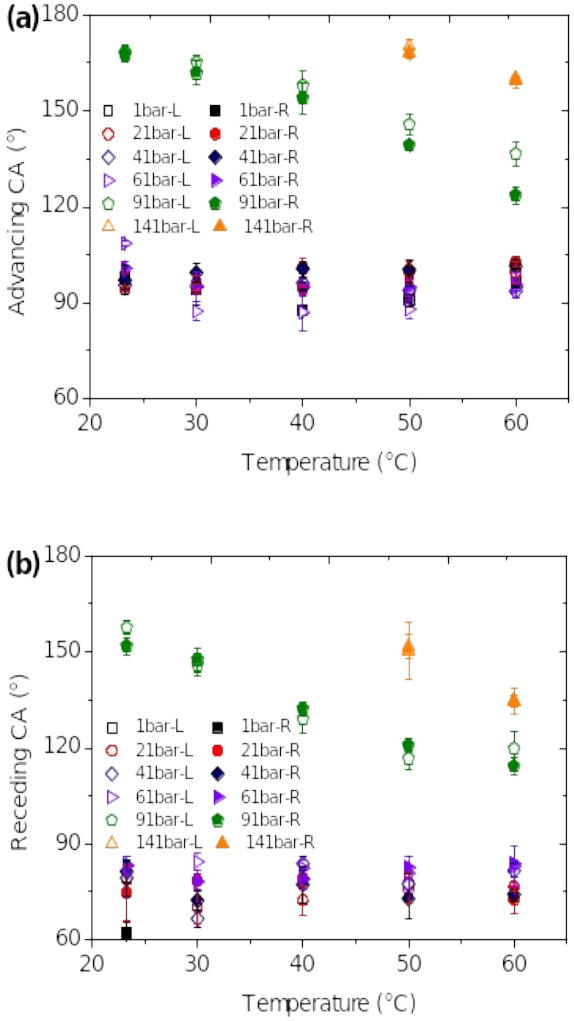

Figure 8 Measured pressure and temperature dependence of DCAs. “L” and “R” refer to measured values on the left and right sides of the bubble, respectively. Range bars represent standard deviations.

At the higher pressures of 91 bar and 141 bar, the coal became strongly CO_2-wet and the DCAs became very large. At these higher pressures, both the advancing and receding contact angles decreased significantly with increased temperature. At room temperature (~25 °C), the mean advancing and receding contact angles at 91 bar are as large as 168° and 155°, respectively. The dynamic contact angles at 141 bar were much larger than those at 91 bar, and they are even as high as ~180° when the temperature

decreased to 40 °C and lower. Arif et al. reported a similar trend in their experiments (Arif, et al., 2016), i.e. both the advancing and receding contact angles slightly decreased with temperature (35, 50, and 70 °C) and increased with pressure.

4 Discussion

4.1 Comparisons of our measured contact angles with the literature values

Figure 9 summarizes static contact angles measured by some previous researchers. Coal types of the samples used in their experiments varied from bituminous coal to anthracite coal. Proximate analysis results of these coal samples mentioned in the literatures were given in Table 2. A comparison between our measurements and previous results was made and the main findings are as follows:

(1) Our findings are similar to the overall increasing trend of SCAs with increased pressure of CO_2 bubbles reported in the literatures. This trend was also found in other types of rocks (Ameri, et al., 2013; Iglauer, et al., 2014; Wan, et al., 2014).

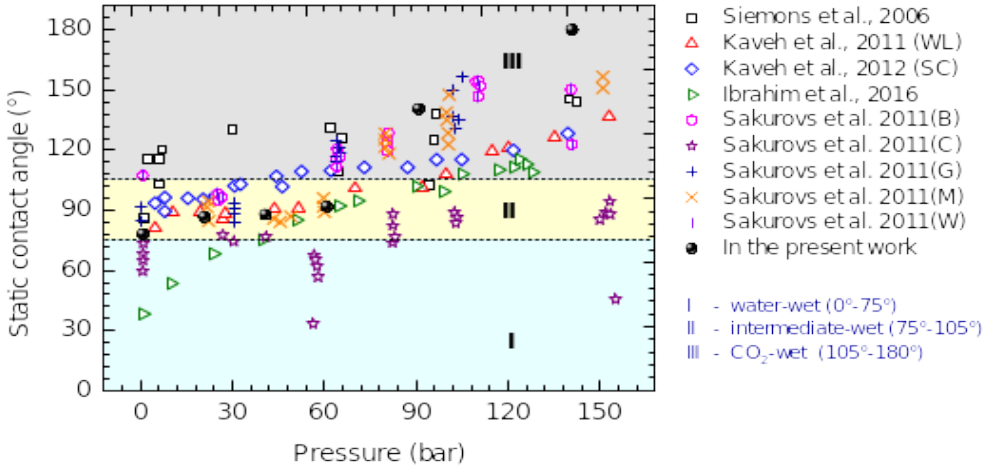

Figure 9. Comparison of static contact angles (measured from water phase) on the coal surfaces in the literatures with that from the present work. □, △, ◇, ▷, ●, contact angles were measured from water phase. ○, ☆, ▯, ×, |, contact angles were measured from CO_2 phase (θ_{CO2}) and converted here to SCAs measured through water by equation (180-θ_{CO2}). WL, SC, B, C, G, M, and W are symbols indicating coal types in the literatures.

Table 2 Proximate analysis results of coal samples given in the literatres.

Literature	Moisture (%)	Ash (%)	Volatile (%)	Carbon (%)	Rmax (%)	*t* (°C)	Coal type
Siemons et al., 2006	1.3	3.9	10.4	85.68	2.41	45	anthracite
Kaveh et al., 2011 (WL)	N/A	2.77	40.5	58.36	0.71	45	hvbB
Kaveh et al., 2012 (SC)	N/A	3.94-5.5	10.4	89.27	2.41	45	semi-anthracite
Ibrahim et al., 2016	0.2	2	47	50.8	N/A	40	hvAb
Sakurovs et al., 2011 (B)	N/A	7.7	31.7	83.0	0.69	40	N/A
Sakurovs et al., 2011 (C)	N/A	20.3	31.2	80.7	0.62	40	N/A
Sakurovs et al., 2011 (G)	N/A	5.6	36.1	84.1	0.95	40	N/A
Sakurovs et al., 2011 (M)	N/A	16.9	21.7	88.9	1.4	40	N/A
Sakurovs et al., 2011 (W)	N/A	8.9	24.3	88.4	1.31	40	N/A
In the present work	8.68	10.6	35.36	57.79	0.49	40	Sub-bituminous

* hvbB = high volatile bituminous coal, hvAb = high volatile A bitumen coal, N/A = not available.

(2) Although most coals were intermediate-wet or CO_2-wet (except Ibrahim et al (Ibrahim and Nasr-El-Din, 2016) and Sakurovs et al's experiments (Sakurovs and Lavrencic, 2011)), the SCAs measured by different researchers are quite different, even at the same pressure and similar temperature. For example, the SCAs varied from ~30° to ~ 120° at atmospheric pressure, indicating that the coals varied from water-wet to CO_2-wet. The primary reasons are attributable to differences in coal types as shown in Table 2. The treatment of the coal surface may be another important factor. Kaveh et al. and Siemons et al. polished the coal surface using a series of abrasive papers (60 to 1200 grid) and 0.5-μm abrasive alumina powder as mentioned above (Kaveh, et al., 2011; Kaveh, et al., 2012; Siemons, et al., 2006), and Ibrahim et al polished the coal surface using a series of sandpapers with average particle diameter 35, 58.5, 100, and 125μm) (Ibrahim and Nasr-El-Din, 2016). Sakurovs polished with a worn P220 silicon carbide paper (Sakurovs and Lavrencic, 2011). The experiment procedures may be different as well, and can contribute to the differences in experimental results. The SCAs in the experiments of Ibrahim et al. (2016) and

Sakurovs et al. (2011) were measured from CO_2 bubbles that were released from the injection needle and buoyantly rose up to the coal surfaces. Siemons et al. (2006) let the CO_2 bubble grow until it hit coal surfaces and then measured the SCAs (the bubble contacted on both the needle and the coal surface during the process).

(3) The coal type used in our experiments is similar to that used by Kaveh et al. (Kaveh, et al., 2011), and the SCAs are also similar when CO_2 is in the gas phase. However, the SCAs increased more dramatically when CO_2 became supercritical in our experiments. Our results are more similar to those in Sakurovs et al's experiments despite the large differences in the coal types (Sakurovs and Lavrencic, 2011), i.e. the SCAs showed a slight increase when CO_2 is in the gas phase and followed by a sharp increase when CO_2 became supercritical.

DCAs on coal surfaces have seldom been reported in the literature, with the exception of the recent work by Arif et al. (Arif, et al., 2016). A comparison of DCAs obtained in our experiments with theirs is shown in **Figure 10**. The DCAs from both studies increased with pressures and were close in gas CO_2 phase, except for the nearly constant advancing contact angles in the present work. When the CO_2 became supercritical, the DCAs in our experiments kept increasing until up to ~180°. However, the DCAs obtained by Arif et al. tended to stabilize, indicating a weaker CO_2 wettability.

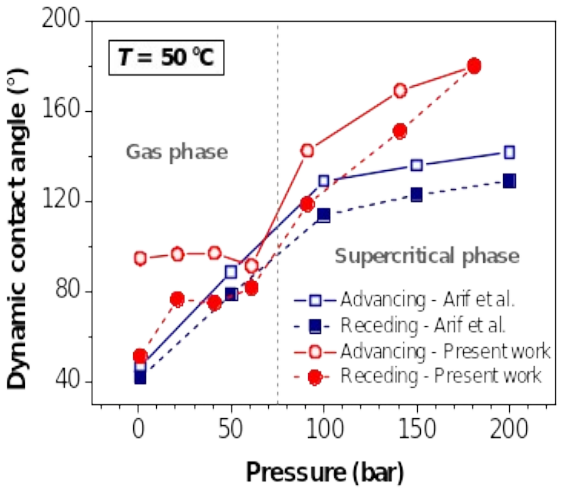

Figure 10. Comparison of pressure-dependence of DCAs measured by Arif et al (2016) with that from the present work. The vertical dashed line indicates the critical pressure for CO_2 (73.8 bar).

4.2 Effect of temperature on contact angles

In our experiments, both the SCAs and DCAs decreased distinctly with increase of temperature when the CO_2 became supercritical.

Villa et al. proposed a model derived from the Decreasing Trend Model for polar liquid (water in the present work) developed by Owens and Wendt (Owens and Wendt, 1969) to calculate the contact angle (Villa, et al., 2018):

$$\cos(\theta) = -1+\frac{2}{\sqrt{\gamma_{LV,0}(1-aT)}}\sqrt{c} \quad (20\ ^\circ C < T < 90\ ^\circ C) \tag{1}$$

Where, θ is the contact angle; $\gamma_{Lv,0}$ is the surface tension of water at a reference temperature T_0 (normally T_0 = 20 °C); a is the temperature coefficient that is positive for one phase substance; c can be calculated by:

$$c=\sqrt{\gamma_{sg}^{D}\frac{\gamma_{lg}^{D}}{\gamma_{lg}}+\gamma_{sg}^{P}\frac{\gamma_{lg}^{P}}{\gamma_{lg}}} \tag{2}$$

where γ_{sg} and γ_{lg} are solid–gas interfacial tension and liquid–gas interfacial tension, respectively, D is the dispersion force (van der Waals interaction) and P is the combined polar force (e.g. dipole-dipole interactions and hydrogen bonding). Due to the negligible variation of γ_{sg} and γ_{sl} in the temperature range 20 °C<T<90°C, the c is considered constant (Frolov and Mishin, 2009; Villa, et al., 2018). Thus, the temperature T is the only variable term in the formula. Therefore, the contact angle (always in the range of 0° to 180°) will decrease with the increase of the experiment temperature.

At constant pressure, the intermolecular distance among H_2O molecules will be enlarged due to the increase of temperature, which weakens the intermolecular attraction ($F_{H2O\text{-}H2O}$) among H_2O molecules on the interface between H_2O phase and CO_2 phase (**Figure 11**). Meanwhile, the intermolecular attraction between CO_2 and H_2O molecule ($F_{CO2\text{-}H2O}$) decreases. The surface tension of water–CO_2 will decrease as a result. This has been experimentally validated by many researchers. For example, the surface tension of water at 25, 30, 40, 50, and 60 °C under atmospheric pressure is 71.99×10^{-3}, 71.20×10^{-3}, 69.60×10^{-3}, 67.94×10^{-3}, and 66.24×10^{-3} N/m, respectively (Vargaftik, et al., 1983), which shows a slight decrease as temperature is increased. Thus, the contact angle on a given solid surface will also decrease with increased temperature at constant pressure. Meanwhile,

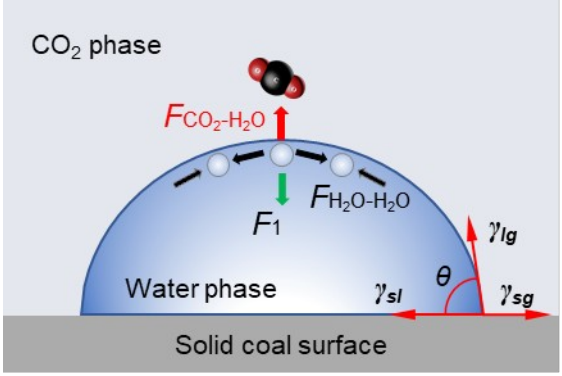

Figure 11 Schematic of the relationship between the contact angle, interfacial tension, and intermolecular attraction or force (IMF). $F_{CO_2\text{-}H_2O}$ is the IMF between CO_2 and H_2O molecule at water□CO_2 interface, and $F_{H_2O\text{-}H_2O}$ is the IMF among H_2O molecules. F_1 is the inward force due to missing cohesive forces to neighboring H_2O molecule, which is directed toward the internal water.

However, the contact angles showed no obvious decreases with increasing temperature at pressures below 61 bar. **Figure 12** gives pressure-dependent CO_2 density for the present experimental conditions. The gas CO_2 densities at different temperatures are very close for pressures below 61 bar. Thus, the $F_{CO_2\text{-}H_2O}$ differs little with temperature, and the surface tension of water–CO_2 will not vary much. This explains why the effect of temperature on contact angles was minor at pressures below 61 bar. The differences in scCO_2 densities among different temperatures become larger as the pressure increased, which led to a more obvious decrease of temperature-dependent contact angles.

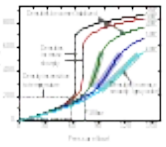

Figure 12 Pressure-dependence of CO_2 density for different temperatures. Calculated with "Thermophysical Properties of Fluid

Systems" in NIST Chemistry WebBook, NIST Standard Reference Database Number 69 (Lemmon, et al., 2018).

4.3 Effect of pressure on contact angles

The above results show that both static and dynamic contact angles increased slightly at pressures below 61 bar and showed a distinct increase when CO_2 transformed from gas phase to liquid and supercritical phase. When the pressure increases, the density of the CO_2 phase will increase, which magnifies the intermolecular attraction forces $F_{CO_2\text{-}H_2O}$ and $F_{H_2O\text{-}H_2O}$ (**Figure 11**). Given that the change in water density is small in our experimental condition (Cho, et al., 2002), the contact angle will then increase as a result. This phenomenon is not obvious at low pressures, but it will be more significant at high pressures.

Some researchers also suggested that the effect of pressure on contact angles was mainly related to the variation in CO_2 density (Arif, et al., 2016; Kaveh, et al., 2011; Kaveh, et al., 2012). **Figure 13** gives the pressure-dependence of advancing and receding CAs (average values of the left and right DCAs) at different temperatures. It shows that there is a good correspondence between CO_2 densities and the DCAs as shown in subordinate figures in **Figure 13** (25 °C for example).

(1) When the pressure is lower than 61 bar, the CO_2 densities increase smoothly as shown in Figure 12, and they are very close at different temperatures varying from ~25 °C to 60 °C. The advancing CAs shows no obvious increase, while the receding CAs indicates a slight increase.

(2) As the pressure rises above 61 bar, the CO_2 densities increase sharply, especially at the lower temperatures. This explains why the differences in the contact angles between lower pressures (1, 21, 41, 61 bar) and larger pressures (91 bar and 141 bar) are larger as shown in **Figure 13**.

(3) When the pressure keeps increasing, the CO_2 densities for different temperatures become stabilized. When the pressure is larger than 141 bar in our experiments, the contact angles in **Figure 7** and **Figure 13** became very large or even increase up to 180° at lower temperatures, indicative of stable hydrophobic conditions. The stabilized pressure also depends on temperature and solid surface types. For example, in the experiments of Arif. et al., the DCAs showed a distinct flatness when the pressure was larger than ~100 bar (Arif, et al., 2017). Espinoza et al. found that the contact angles on both hydrophobic substrates (oil-wet quartz and PTFE) and hydrophilic substrates (quartz and calcite) remained

constant after the pressure exceeds the CO_2 liquid-vapor phase boundary (~64.33 bar at 298K) (Espinoza and Santamarina, 2010).

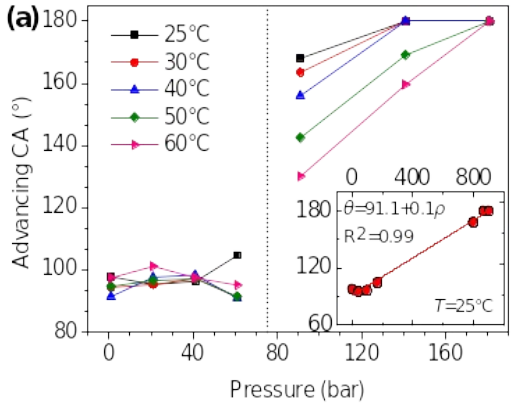

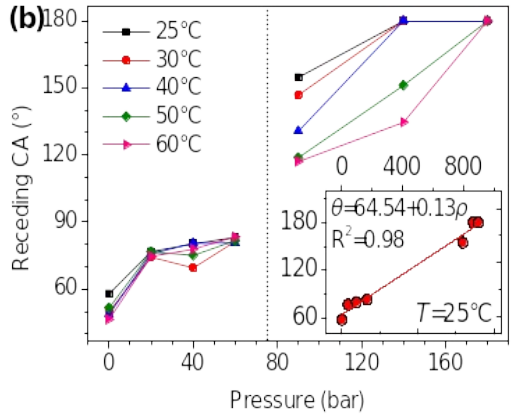

Figure 13. Pressure-dependence of the advancing and receding DCAs at different temperatures. The vertical dashed line indicates the critical pressure for CO_2 (73.8 bar). The abscissa of the subordinate figure is the CO_2 density (ρ, kg·m^{-3}), and the ordinate is the dynamic contact angle (θ).

As discussed in previous section, when the pressure increases, CO_2 adsorption on coal surfaces is enhanced, which also leads to the decrease of interfacial tension between CO_2 and the solid surface, and the increase in contact angles (Espinoza and Santamarina, 2010; Ibrahim and Nasr-El-Din, 2016). However, this may be not as significant as the effect of CO_2 density variation. In our experiments, the coal sample was completely immersed in water, and water molecules occupied most of the adsorption sites on the coal surfaces before the CO_2 bubble contact. As is known, water has higher adsorption capacity than CO_2 (Merkel, et al., 2015), so the coal surface sites will uptake low amounts of CO_2 during the contact

process, especially within short times. Further studies are needed to measure CO_2 uptake amount on water-immersed coal surfaces at different pressures and temperatures.

5 Conclusions

We experimentally investigated the wettability of coals by measuring both static and dynamic contact angles over wide ranges of pressures and temperatures. The main findings are as follows:

(1) The coal surface is weakly water-wet (57˚) before contacting with CO_2. The reactions with gas-CO_2 slightly altered the coal surfaces to become intermediate-wet (SCAs increased to 70°-90°). The reactions with scCO_2 strongly altered the coal surfaces to become CO_2-wet (~115-180˚).

(2) The effect of temperature on both static and dynamic contact angles is negligible in gas-CO_2. However, when the pressure increased above the critical pressure, the contact angles decreased with the increased temperature.

(3) For gas-CO_2, both static and dynamic contact angles increased slightly with increase of pressures. For liquid-CO_2 and scCO_2, the static and dynamic contact angles on coal surface increased greatly with the increase of pressures.

(4) The contact angles for water on coals were strongly positively correlated to CO_2 densities.

Acknowledgement

Financial support provided by the National Natural Science Foundation of China (NSFC) (Grant Number: 51874293) and National Science and Technology Major Project (Grant Number: 2018YFC0807905) for this research is gratefully acknowledged. JW and TKT were supported by the U.S. Department of Energy, Office of Fossil Energy, Office of Natural Gas and Petroleum Technology, through the National Energy Technology Laboratory (NETL), and Office of Basic Energy Sciences, Chemical Sciences, Geosciences, and Biosciences Division under Award Number DE-AC02-05CH11231 and FWP-ESD14085.

References

Specification for Identification of Coal and Gas Outburst Coal Mine. In: Safety, S.A.o.W., editor. Beijing: China Coal Industry Publishing House; 2006.

Notice on speeding up the closure and withdrawal of small coal mines. In: State Administration of Work Safety, N.C.M.S.A., National Development and Reform Commission, Ministry of Public Security, Ministry of Finance,

Ministry of Human Resources and Social Security, Ministry of Land and Resources, Ministry of Environmental Protection, State-owned Assets Supervision and Administration Commission, State Administration for Industry and Commerce, National Energy Administration, All-China Federation of Trade Unions, editor. Beijing; 2014.

Ameri, A.*, et al.* Investigation on Interfacial Interactions among Crude Oil−Brine−Sandstone Rock−CO_2 by Contact Angle Measurements. *Energy & Fuels* 2013;27:1015−1025.

Anderson, W.G. Wettability literature survey - Part 2: Wettability measurement. *Journal of Petroleum Technology* 1986;38(11):1246-1262.

Arif, M.*, et al.* CO_2-wettability of low to high rank coal seams: Implications for carbon sequestration and enhanced methane recovery. *Fuel* 2016;181:680-689.

Arif, M.*, et al.* Influence of surface chemistry on interfacial properties of low to high rank coal seams. *Fuel* 2017;194:211-221.

Bhutani, G., Khandekar, S. and Muralidhar, K. Contact Angles of Pendant Drops on Rough Surfaces. In, *Proceedings of the Thirty Ninth National Conference on Fluid Mechanics and Fluid Power*. Gujarat, India: SVNIT Surat; 2012. p. 1-10.

Bikkina, P.K. Contact angle measurements of CO_2–water–quartz/calcite systems in the perspective of carbon sequestration. *International Journal of Greenhouse Gas Control* 2011;5:1259–1271.

Busch, A. and Gensterblum, Y. CBM and CO_2-ECBM related sorption processes in coal: A review. *International Journal of Coal Geology* 2011;87:49–71.

Chen, C.*, et al.* Water contact angles on quartz surfaces under supercritical CO_2 sequestration conditions: Experimental and molecular dynamics simulation studies. *International Journal of Greenhouse Gas Control* 2015;42:655-665.

Cho, C.H.*, et al.* Pressure Effect on the Density of Water. *The Journal of Physical Chemistry A* 2002;106:7557-7561.

Drelich, J. Guidelines to measurements of reproducible contact angles using a sessile-drop technique. *Surface Innovations* 2013;1(4):248-254.

Drelich, J.*, et al.* Preparation of a coal surface for contact angle measurements. *Journal of Adhesion Science and Technology* 1997;11(11):1399-1431.

Eissler, R.L. and Holde, K.E.V. Wettability of coal, graphite, and Naphthalene as measured by contact angles. In. Urbana: Illinois State Geological Survey 1962.

Espinoza, D.N. and Santamarina, J.C. Water-CO_2-mineral systems: Interfacial tension, contact angle, and diffusion—Implications to CO_2 geological storage. *Water Resoures Research* 2010;46(7).

Frolov, T. and Mishin, Y. Temperature dependence of the surface free energy and surface stress: An atomistic calculation for Cu(110). *Physical review B* 2009;79(4):045430.

Gunter, W.D.*, et al.* Deep coalbed methane in Alberta, Canada: A fuel resource with the potential of zero greenhouse gas emissions. *Energy Conversion and Management* 1997;38(Supplement):S217-S222.

Ibrahim, A.F. and Nasr-El-Din, H.A. Effect of Water Salinity on Coal Wettability During CO_2 Sequestration in Coal Seams. *Energy & Fuels* 2016;30:7532−7542.

Iglauer, S.*, et al.* Contamination of silica surfaces: Impact on water–CO_2–quartz and glass contact angle measurements. *International Journal of Greenhouse Gas Control* 2014;22:325–328.

Jańczuk, B., Wójcik, W. and Bialopiotrowicz, T. Wettability of Coal Surface and its Surface Free Energy Components. *Croatica Chemica Acta* 1988;61(1):51-63.

Jung, J.W. and Wan, J. Supercritical CO_2 and Ionic Strength Effects on Wettability of Silica Surfaces: Equilibrium Contact Angle Measurements. *Energy & Fuels* 2012;26:6053−6059.

Kaveh, N.S.*, et al.* Wettability determination by contact angle measurements: hvbB coal–water system with injection of synthetic flue gas and CO_2. *Journal of Colloid and Interface Science* 2011;364:237–247.

Kaveh, N.S.*, et al.* Effect of coal petrology and pressure on wetting properties of wet coal for CO_2 and flue gas storage. *International Journal of Greenhouse Gas Control* 2012;11(Supplement):S91-S101.

Kilau, H.W. The wettability of coal and its relevance to the control of dust during coal mining. *Journal of Adhesion Science and Technology* 1993;7(6):649-667.

Lemmon, E.W., McLinden, M.O. and Friend, D.G. Thermophysical Properties of Fluid Systems. In. Gaithersburg MD: National Institute of Standards and Technology; 2018.

Letellier, P., Mayaffre, A. and Turmine, M. Drop size effect on contact angle explained by nonextensive thermodynamics. Young's equation revisited. *Journal of Colloid and Interface Science* 2007;314:604–614.

Leung, D.Y.C., Caramanna, G. and Maroto-Valer, M.M. An overview of current status of carbon dioxide capture and storage technologies. *Renewable and Sustainable Energy Reviews* 2014;39:426–443.

Mahoney, S.A.*, et al.* The effect of rank, lithotype and roughness on contact angle measurements in coal cleats. *International Journal of Coal Geology* 2017;179:302-315.

Marmur, A. Soft contact: measurement and interpretation of contact angles. *Soft Matter* 2006;2:12–17.

Masoudian, M.S. Multiphysics of carbon dioxide sequestration in coalbeds:

A review with a focus on geomechanical characteristics of coal. *Journal of Rock Mechanics and Geotechnical Engineering* 2016;8:93-112.
Merkel, A.*, et al.* Competitive sorption of CH_4, CO_2 and H_2O on natural coals of different rank. *International Journal of Coal Geology* 2015;150-151:181–192.
Mukherjee, M. and Misra, S. A review of experimental research on Enhanced Coal Bed Methane (ECBM) recovery via CO_2 sequestration. *Earth-Science Reviews* 2018;179:392–410.
Owens, D.K. and Wendt, R.C. Estimation of the Surface Free Energy of Polymers. *journal of Applied Polymer Science* 1969;13:1741-1747.
Pan, B.*, et al.* CO_2 and CH_4 Wettabilities of Organic-Rich Shale. *Energy & Fuels* 2018;32:1914−1922.
Puri, R. and Yee, D. Ehanced coalbed methane recovery. In, *65th Annual Technical Conference and Exhibition*. New Orleans, LA: Society of Petroleum Engineers; 1990.
Saghafi, A., Pinetown, K. and Javanmard, H. Gas Wettability of Coal and Implications for Gas Desorption and Drainage. In, *14th Coal Operators' Conference*. University of Wollongong: The Australasian Institute of Mining and Metallurgy & Mine Managers Association of Australia; 2014. p. 266-273.
Sakurovs, R. and Lavrencic, S. Contact angles in CO_2-water-coal systems at elevated pressures. *International Journal of Coal Geology* 2011;87(1):26-32.
Siemons, N.*, et al.* Pressure dependence of the contact angle in a CO_2–H_2O–coal system. *Journal of Colloid and Interface Science* 2006;297:755–761.
Sun, X.-x.*, et al.* Investigations of CO_2-water wettability of coal: NMR relaxation method. *International Journal of Coal Geology* 2018;188:38–50.
Taggart, A.F., Taylor, T.C. and Ince, C.R. Experiments with Flotation Reagents. *Transactions of the American Institute of Mining, Metallurgical, and Petroleum Engineers* 1930;87:285-289.
Vargaftik, N.B., Volkov, B.N. and Voljak, L.D. International Tables of the Surface Tension of Water. *Journal of Physical and Chemical Reference Data* 1983;12(3):817-820.
Villa, F., Marengo, M. and De Coninck, J. A new model to predict the influence of surface temperature on contact angle. *Scientific Reports* 2018;8(1):6549.
Wan, J., Kim, Y. and Tokunaga, T.K. Contact angle measurement ambiguity in supercritical CO_2–water–mineral systems: Mica as an example. *International Journal of Greenhouse Gas Control* 2014;31:128-137.
Wan, J.*, et al.* Supercritical CO_2 uptake by nonswelling phyllosilicates. *Proceedings of the National Academy of Sciences* 2018;115(5):873-878.

White, C.M., *et al.* Separation and Capture of CO_2 from Large Stationary Sources and Sequestration in Geological Formations—Coalbeds and Deep Saline Aquifers. *Journal of the Air & Waste Management Association* 2003;53:645-715.